Available online at www.sciencedirect.com
SCIENCE DIRECT
ELSEVIER
European Journal of Mechanics B/Fluids 24 (2005) 91–112
EUROPEAN JOURNAL OF MECHANICS B/FLUIDS

Surface waves created by low-frequency magnetic fields

Y. Fautrelle [a], A.D. Sneyd [b,*]

[a] *EPM-Madylam E.N.S.H.M.G. BP 95, 38402, St. Martin d'Hères cedex, France*
[b] *University of Waikato, Private Bag 3105, Hamilton, New Zealand*

Received 10 November 2003; received in revised form 26 May 2004; accepted 29 May 2004

Available online 29 July 2004

Abstract

This paper analyses the effects of a low frequency A.C. magnetic field on the free surface of a liquid metal. The action of the vertical and uniform magnetic field is twofold. First it creates forced standing surface waves which generally exhibit symmetry related to that of the container; second it triggers non-symmetric free surface instabilities superimposed on the forced regime. A previous paper considered the case of a circular cylindrical tank where axisymmetric forced standing waves caused an electric current perturbation which then excited non-axisymmetric waves at a critical A.C. field intensity. Nonlinear interaction between the symmetric and non-symmetric modes was not taken into account. The present work treats the problem from a more general standpoint. Equilibrium perturbations are developed systematically to order $\mathfrak{N}^2$ (where $\mathfrak{N}$ is the magnetic interaction parameter) and at this level of approximation we also need to consider nonlinear mode interactions and electromagnetic damping. The theory applies to tanks of arbitrary shape and the $O(\mathfrak{N})$ irrotational motion may be described by the torsion function for the particular pool cross-section. For circular and annular tanks we then derive a system of coupled Mathieu–Hill equations for the time-development of non-symmetric surface modes. Two main types of parametric resonance are predicted, namely the single or combination mode, and the particular type observed may depend on the geometry of the tank. Results of the stability analysis are confirmed by experimental work carried out in mercury pools.

Keywords: MHD; Liquid metal; Alternating fields; Parametric resonance

1. Introduction

A.C. magnetic fields are commonly used in various metallurgical devices for heating and stirring liquid metals. Typical frequencies range from 50 Hz to 10^5 kHz. In that frequency range only the mean part of the Lorentz forces plays a significant role, the liquid metal inertia being too large to respond to the oscillating part of the Lorentz forces. The very low frequency range, i.e. from about 1 to 10 Hz, has been quite recently explored. In this case, it has been shown both experimentally and theoretically that the oscillating part of the electromagnetic forces could generate waves on the free surface of a liquid metal [1,2] (referred to hereafter as GFS). This phenomenon occurs when the magnetic field and the first few normal wave modes have frequencies of the same order. Mercury experiments in a cylindrical tank [1] have revealed two principal types of waves. For weak magnetic fields, axisymmetric quasi-steady waves appear on the free surface. These are directly forced by the alternating part of the electromagnetic forces. It was also found that above a critical magnetic field intensity symmetry-breaking occurred and azimuthal modes developed. Their oscillation frequency in the vicinity of the transition was half that of the electromagnetic force.

* Corresponding author.
E-mail addresses: y.fautrelle@hmg.inpg.fr (Y. Fautrelle), sneyd@waikato.ac.nz (A.D. Sneyd).

0997-7546/$ – see front matter
doi:10.1016/j.euromechflu.2004.05.005

Low-frequency fields are currently used in a number of industrial processes. For example a low frequency pulsed A.C. magnetic field in the continuous casting of steel is able to replace mechanical mold vibrations [3]. Contactless free surface stirring may also be used to accelerate the kinetics of mass transfer in slag-metal refining reactions [4].

A theoretical linear stability analysis has been performed by GFS in cylindrical geometry. This showed the existence of a basic state consisting of forced axisymmetric waves. Moreover their simplified stability analysis showed that non-symmetric modes were governed by a system of generalised Mathieu–Hill equations. Thus the appearance of unstable non-symmetric modes could be attributed to parametric resonance. In GFS parametric forcing arises from the electromagnetic force perturbation due to azimuthal surface waves. Any non-symmetric free surface perturbation alters the flow path of the basic axisymmetric induced current and the resulting electromagnetic force perturbation destabilises the free surface. However, in their analysis GFS ignored the influence of both the axisymmetric wave motion as well as the electric current created by the fluid motion across the magnetic field lines. It turns out that nonlinear interactions with the axisymmetric modes are of the same order of magnitude as the electromagnetic force perturbations. We show later that both are of $O(\mathfrak{N}^2)$, and the former effect is likely to have a significant effect on stability. Furthermore, the magnetic field strength required to trigger the instability is quite high, so we might expect electromagnetic damping to be significant.

The present work is a continuation of previous analysis by GFS, but from a more general standpoint. We use an inner-product method to formulate evolution equations for the wave mode amplitudes, performing a systematic expansion to order $\mathfrak{N}^3$, where $\mathfrak{N}$ is the magnetic interaction parameter. This expansion shows it necessary to consider the two effects mentioned above, omitted in the GFS analysis:

(i) nonlinear interactions between the forced-wave regime and non-symmetric modes;
(ii) electric currents induced by the fluid motion across the magnetic field lines.

The inclusion of these two effects produces results which are significantly different from those of GFS. Field strength is measured by $\mathfrak{N}$ and the critical value of $\mathfrak{N}$ necessary to trigger the growth of a parametrically excited mode is denoted by $\mathfrak{N}_C$. Since effect(i) is destabilising we obtain values of $\mathfrak{N}_C$ which are consistently smaller the corresponding GFS values — in other words we find parametric instabilities much easier to excite. This effect is particularly important when the field frequency is nearly half that of a forced wave; then the forced-wave amplitude becomes very large and non-symmetric modes are triggered by a relatively weak field. On the other hand, magnetic damping, effect (ii), suppresses many unstable modes found by GFS. Indeed one complete class of instabilities entirely disappears.

In section two we establish the equations governing forced surface waves — the first-order basic state. Our method of analysis is formulated for tanks of arbitrary cross-section, and as well as the circular tank we consider rectangular and annular geometries. Then in section three we continue the expansion of the evolution equations to $O(\mathfrak{N})^2$. An important advantage of the inner product method is that the order $\mathfrak{N}^2$ rotational flow does not have to be found explicitly. We then use the nonlinear evolution equation to derive a linear equation describing the growth of non-symmetric modes in cylindrical or annular tanks. Section four is devoted to analysis of results and comparisons between theory and experiment. Conclusions are summarised in section five.

2. First-order analysis

We consider a tank with vertical walls and an arbitrary (but uniform) horizontal cross-section. Our method is most clearly formulated if we make no particular assumptions about the tank cross-section, but later we specialise to cylindrical and annular geometries. The tank contains fluid of density ρ and electrical conductivity σ to a depth h, and a uniform vertical alternating magnetic field

$$\boldsymbol{B} = B_0 \sin(\omega t)\hat{\boldsymbol{z}} \tag{1}$$

is applied (Fig. 1). We assume the fluid incompressible so ρ is constant and

$$\nabla \cdot \boldsymbol{v} = 0,$$

where $\boldsymbol{v}$ is fluid velocity. The time-dependent field induces an electric current in the fluid which interacts with the field to produce a Lorentz force, which stirs the fluid and creates a pattern of standing waves on the free surface.

The first-order analysis is dedicated to the determination of the forced regime. We shall make two approximations throughout: first that the magnetic diffusion time $L^2\mu_0\sigma$ (where L is a typical length scale and μ_0 the permeability of free space) is much larger than an oscillation period — i.e.

$$\omega L^2 \mu_0 \sigma \ll 1, \quad \text{or} \quad R_m^* \ll 1, \tag{2}$$

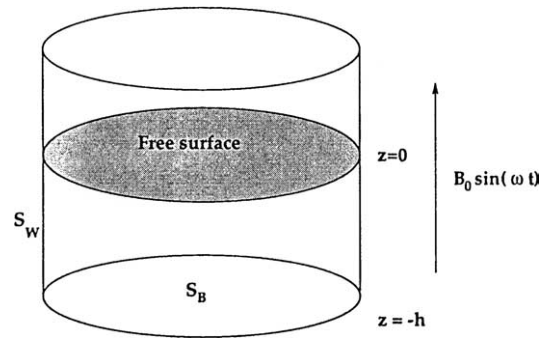

Fig. 1. Sketch of the geometry.

where R_m^* is a magnetic Reynolds number based of the velocity scale ωL. Approximation (2) also means that the magnetic field due to the induced currents is small compared with the applied field, and may be neglected. Our second assumption is that the ratio of electromagnetic to inertia forces is small, which is equivalent to assuming a small interaction parameter,

$$\frac{\sigma B_0^2}{\omega\rho} = \mathfrak{N} \ll 1, \tag{3}$$

as shown in GFS. In the forced-wave regime the induced Lorentz force of order $\sigma\omega L B_0^2$ provides the free-surface acceleration $\omega^2\rho\eta_0$, where η_0 is a typical free-surface displacement. Thus

$$\eta_0 \approx \mathfrak{N}L. \tag{4}$$

$\mathfrak{N}$ will be used as a small expansion parameter.

2.1. The Lorentz force

Combining Faraday's law and Ohm's law,

$$\nabla \times \boldsymbol{E} = -\frac{\partial \boldsymbol{B}}{\partial t}, \qquad \boldsymbol{J} = \sigma(\boldsymbol{E} + \boldsymbol{v} \times \boldsymbol{B}). \tag{5}$$

Note that

$$\left|\frac{\boldsymbol{v} \times \boldsymbol{b}}{E}\right| \text{ is } \mathrm{O}(\mathfrak{N}),$$

so since we have assumed $\mathfrak{N} \ll 1$ we can neglect the induced current $\sigma \boldsymbol{v} \times \boldsymbol{B}$ at this level of approximation. It follows the induced electric current $\boldsymbol{J}$ satisfies,

$$\nabla \times \boldsymbol{J} = -\sigma\omega B_0 \cos(\omega t)\hat{\boldsymbol{z}}. \tag{6}$$

If we make the usual MHD approximation that $\boldsymbol{J}$ is solenoidal, and assume the container walls to be insulating, then $\boldsymbol{J}$ must also satisfy

$$\nabla \cdot \boldsymbol{J} = 0, \qquad \boldsymbol{J} \cdot \hat{\boldsymbol{n}} = 0 \quad \text{on } \partial V. \tag{7}$$

Here ∂V is the closed surface bounding the volume V of conducting fluid, comprising the tank walls, base, and free surface, and $\hat{\boldsymbol{n}}$ is the outward unit vector normal to ∂V.

Eq. (4) shows in calculating the electric current to order $\mathfrak{N}$ we may assume the free surface horizontal. In this case the induced electric current is also purely horizontal and independent of the vertical co-ordinate z, so there is no build-up of electric charge on the free surface. It also follows that $\boldsymbol{J}$ can be represented by a flux function $G(x, y)$,

$$\boldsymbol{J} = \nabla G \times \hat{\boldsymbol{z}}, \qquad G = \text{constant on } C, \tag{8}$$

where C is a curve in the (x, y)-plane corresponding to the cylinder walls. Since quantities of interest depend only on the *gradient* of G we can choose the constant to be zero, provided the region is simply connected. The form (8) satisfies Eqs. (7) identically, and (6) will also be satisfied provided

$$\nabla^2 G = \sigma\omega B_0 \cos(\omega t). \tag{9}$$

The solution is therefore,

$$G = -\sigma\omega B_0 \cos(\omega t) T(x, y), \tag{10}$$

where $T(x, y)$ is the *torsion function* for the interior of the closed curve C — i.e. T is the solution of the boundary-value problem

$$\nabla^2 T = -1, \qquad T = 0 \quad \text{on } C. \tag{11}$$

The problem (11) arises in the elastic theory of twisted rods [5, §16] and also in the theory of Poiseuille flow [6]. For a number of simple cross-section geometries T is given by an analytic formula; for the circle $r = a$,

$$T = \frac{1}{4}\left(a^2 - r^2\right),$$

and for the ellipse $x^2/a^2 + y^2/b^2 = 1$,

$$T = \frac{a^2 b^2}{a^2 + b^2}\left(1 - \frac{x^2}{a^2} - \frac{y^2}{b^2}\right).$$

Multiply-connected regions require a slightly more detailed analysis, since G may take *different* constant values on different boundaries. In particular we need to consider an annular tank $a \leqslant r \leqslant b$ (cylindrical polars). Since

$$\boldsymbol{A} = \frac{1}{2}\omega B_0 \cos(\omega t) r\,\hat{\boldsymbol{\theta}}$$

is a vector potential for $\partial \boldsymbol{B}/\partial t$, it follows from the first of Eqs. (5) that

$$\boldsymbol{E} = -\boldsymbol{A} + \nabla\phi,$$

where ϕ is an arbitrary function. Taking the divergence of this equation and noting that $\boldsymbol{J}\cdot\hat{\boldsymbol{n}} = 0$ on the walls $r = a,\ r = b$ we conclude that,

$$\nabla^2\phi = 0, \qquad \nabla\phi\cdot\hat{\boldsymbol{n}} = \boldsymbol{A}\cdot\hat{\boldsymbol{n}}, \quad \text{on } r = a,\ r = b.$$

It follows that $\phi = 0$, $\boldsymbol{E} = -\boldsymbol{A}$, $\boldsymbol{J} = -\sigma\boldsymbol{A}$ and

$$T = -\frac{1}{4}r^2. \tag{12}$$

The Lorentz force can be found using (8) and (9):

$$\boldsymbol{J}\times\boldsymbol{B} = (\nabla G\times\hat{\boldsymbol{z}})\times B_0\sin(\omega t)\hat{\boldsymbol{z}} = \frac{1}{2}\sigma\omega B_0^2\sin(2\omega t)\nabla T. \tag{13}$$

This force field is irrotational, so for large Reynolds numbers the velocity field $\boldsymbol{v}$ will be irrotational (except in thin viscous boundary layers on the cylinder walls).

2.2. The free surface expansion

To describe the free-surface displacement it is convenient to follow Wang [7] and introduce the functions $E_n(x, y)$, $n = 1, 2, \ldots$, which are the eigenfunctions of the problem,

$$\nabla^2 E_n + \lambda^2 E_n = 0, \qquad \nabla E_n\cdot\hat{\boldsymbol{n}} = 0 \quad \text{on } C. \tag{14}$$

Note that integrating this equation over the tank cross-section shows

$$\int E_n\,\mathrm{d}x\,\mathrm{d}y = 0.$$

The free surface displacement η is then expanded in the form

$$\eta = \sum_{n=1}^{\infty} a_n(t) E_n, \tag{15}$$

where the a_n are functions of time to be determined. Although the eigenfunctions are necessarily real they may be written in complex form for ease of manipulation, in which case the a_n will also be complex. For example the circular cylinder eigenfunctions can be written in the form

$$\mathrm{e}^{\mathrm{i}m\theta} J_m(\lambda_{mn} r), \tag{16}$$

where λ_{mn} the n-th zero of $J'_m(\lambda a)$. To ensure that the free surface displacement η is real, the coefficients corresponding to the eigenfunctions $J_m(\lambda_{mn} r)\,\mathrm{e}^{\pm \mathrm{i}m\theta}$ must be complex conjugates. For the annulus, the eigenfunctions are

$$\mathrm{e}^{\mathrm{i}m\theta}\, y_{mn}(r),$$

where $y_{mk}(r)$ is the n-th eigenfunction of the eigenvalue problem,

$$r^2 y'' + r y' + \left(\lambda^2 r^2 - m^2\right) y = 0; \quad y'(a) = y'(b) = 0.$$

The functions E_n form an orthogonal sequence:

$$\int E_n E_q^* \,\mathrm{d}x\,\mathrm{d}y = \delta_{nq} \|E_n\|^2; \qquad \int \nabla E_n \cdot \nabla E_q^* \,\mathrm{d}x\,\mathrm{d}y = \delta_{nq} \lambda_n^2 \|E_n\|^2, \tag{17}$$

where

$$\|E_n\|^2 = \int_V E_n E_n^* \,\mathrm{d}V,$$

the asterisk denoting the complex conjugate. We also define a related sequence of harmonic functions, by setting

$$\phi_n(x, y, z) = \frac{\cosh \lambda_n (z + h) E_n(x, y)}{\lambda_n \sinh \lambda_n h} = E_n(x, y) f_n(z) \ \text{ say.} \tag{18}$$

These functions satisfy

$$\nabla^2 \phi_n = 0, \qquad \nabla \phi_n \cdot \hat{\boldsymbol{n}} = 0 \quad \text{on } S_W \text{ and } S_B, \qquad \left(\frac{\partial \phi}{\partial z}\right)_{z=0} = E_n, \tag{19}$$

where S_W is the vertical cylinder wall and S_B the cylinder base.

2.3. Evolution equations

The linearised Euler equation of motion is

$$\rho \frac{\partial \boldsymbol{v}}{\partial t} = -\nabla P + \boldsymbol{J} \times \boldsymbol{B}. \tag{20}$$

Here $P = p + \rho g z$, where p is the fluid pressure. We neglect surface tension, so on the free surface $p = 0$ and the linearised boundary conditions are:

$$(P)_{z=0} = \rho g \eta, \qquad \dot{\eta} = (v_z)_{z=0}. \tag{21}$$

We define the *inner product* of two vector fields as

$$\langle \boldsymbol{A}, \boldsymbol{B} \rangle = \int_V \boldsymbol{A} \cdot \boldsymbol{B}^* \,\mathrm{d}V,$$

and derive evolution equations for the $a_n(t)$ by taking the inner product of (20) with each of the test functions $\nabla \phi_n$ [7]. The first term, for example gives

$$\rho \langle \dot{\boldsymbol{v}}, \nabla \phi_n \rangle = \rho \int_V \nabla \cdot (\phi_n^* \dot{\boldsymbol{v}}) \,\mathrm{d}V = \int_S \phi_n^* \dot{v}_z \,\mathrm{d}x\,\mathrm{d}y,$$

where S is the free surface $z = 0$ (assumed plane to order $\mathfrak{N}$). We have used Gauss's Theorem, the tank walls and base, on which $\boldsymbol{v} \cdot \hat{\boldsymbol{n}} = 0$ giving no contribution to the resulting surface integral. Using the second of Eqs. (21) and the orthogonality of the eigenfunctions, this simplifies to:

$$\rho \langle \dot{\boldsymbol{v}}, \nabla \phi_n \rangle = f_n(0) \int_S E_n^* \ddot{\eta} \,\mathrm{d}x\,\mathrm{d}y = \frac{1}{\lambda_n T_n} \|E_n\|^2 \ddot{a}_n, \tag{22}$$

where

$$T_n = \tanh(\lambda_n h).$$

The two other terms are dealt with similarly and we obtain the following evolution equation:

$$\ddot{a}_n + \Omega_n^2 a_n = \frac{1}{2} \omega^2 \mathfrak{N} \lambda_n \Gamma_n T_n \sin(2\omega t), \quad \Omega_n^2 = g \lambda_n T_n. \tag{23}$$

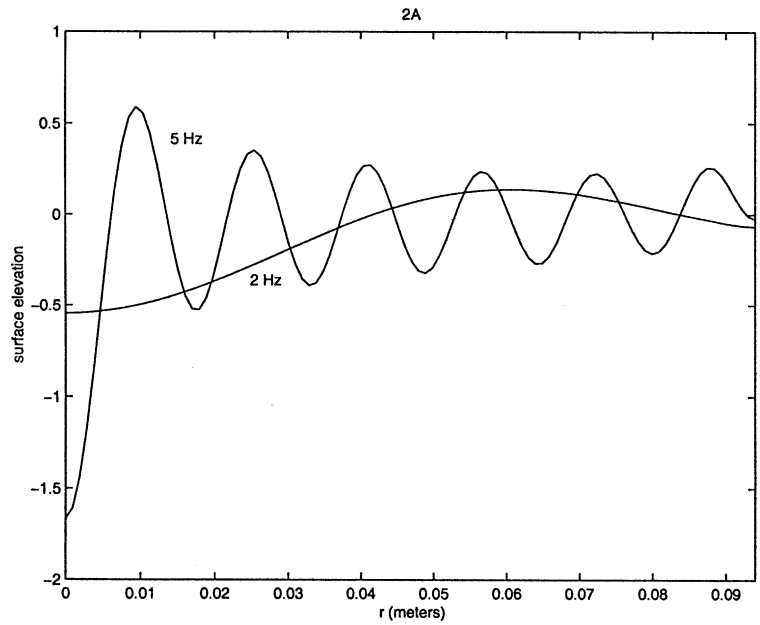

Fig. 2. Forced-wave displacement in a circular mercury tank of radius 0.095 m for two applied frequencies. The elevation $\eta/(\mathfrak{N}\sin(2\omega t))$ is plotted.

The frequencies Ω_n are just the natural gravity-wave frequencies; the coefficient Γ_n represents the force arising from the induced current, and is defined in the appendix.

When the applied field has been switched on for a long time, so that transient solutions of (23) have decayed sufficiently (e.g. under the influence of viscous or ohmic dissipation not included in this $O(\mathfrak{N})$ analysis) a periodic solution proportional to $\sin(2\omega t)$ will be established;

$$\eta = \sum_{n=1}^{\infty} E_n a_n(t), \quad a_n(t) = \mathfrak{N} h_n \sin(2\omega t), \tag{24}$$

where the h_n coefficient is defined in Appendix A. For the circular cylinder,

$$\eta = \frac{1}{8}\mathfrak{N}\sin(2\omega t)\sum_{n=1}^{\infty} \frac{T_n J_0(\lambda_{0n} r)}{\lambda_{0n} J_0(\lambda_{0n} a)[1 - (\Omega_n^2/4\omega^2)]}, \tag{25}$$

which is identical to Eq. (2.18) of GFS. The torsion function for the circular cylinder is axisymmetric, so from (16) we see that $\Gamma_n = 0$ except for the $m = 0$ modes. Thus only eigenfunctions of the form $J_0(\lambda_{0k} r)$ appear in the expansion (24), and the surface waves form circular concentric ripples. A comparison given in GFS with experimental results shows good agreement. Fig. 2 shows free-surface profiles in an cylindrical tank for two excitation frequencies. Fig. 3 shows a photograph of the experimental forced wave regime in a cylindrical tank.

The flow, being irrotational is determined uniquely by the specification of $v_z(x, y)$ on the free surface. It follows that

$$\boldsymbol{v} = \sum_{n=1}^{\infty} \dot{a}_n \nabla\phi_n + O(\mathfrak{N}^2). \tag{26}$$

In this section we used an approximation of order zero in $\mathfrak{N}$ for the free-surface displacement η to find the improved approximation (25) which is $O(\mathfrak{N})$. In the next section, to describe the growth of non-axisymmetric modes, we use our $O(\mathfrak{N})$ expressions for η and $\boldsymbol{v}$ to derive a mode-evolution equation accurate to $O(\mathfrak{N}^2)$.

3. Analysis to order $\mathfrak{N}^2$

Galpin and Fautelle [1] found in their experiment with a circular tank that for sufficiently strong magnetic fields, non-axisymmetric modes were excited. This observation implies that the forced-wave solution for the circular tank (25) may become

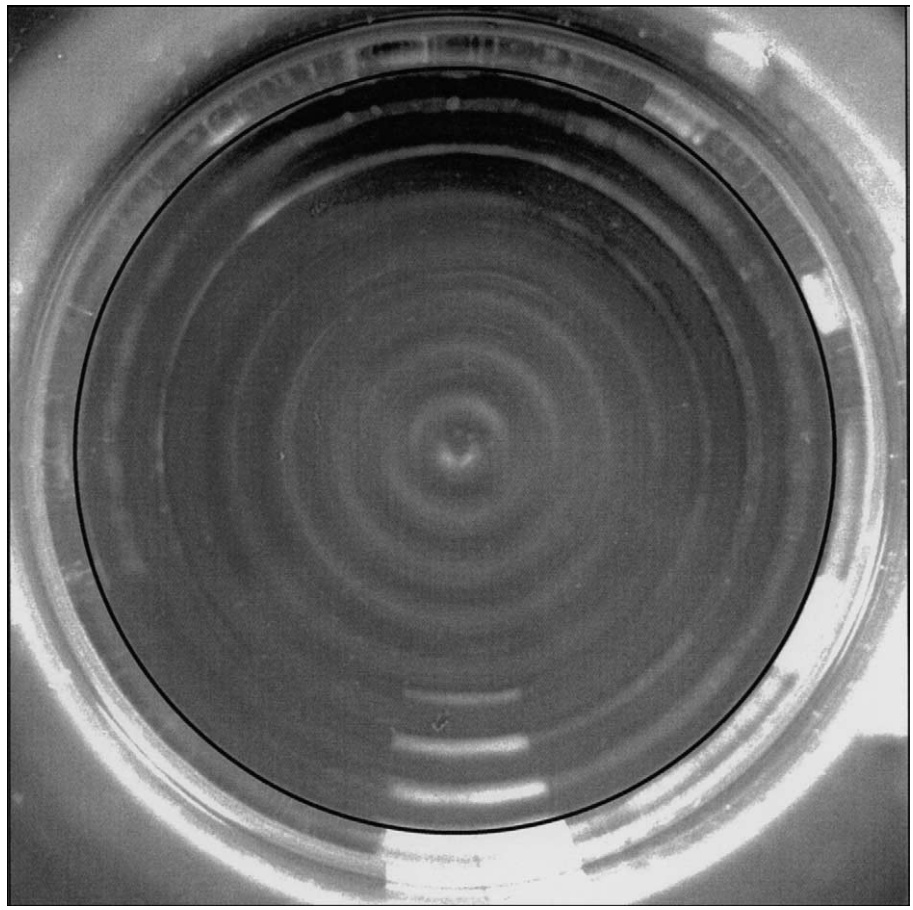

Fig. 3. Axisymmetric forced-wave pattern in a cylindrical tank [1]. The dominant mode is (0,15) with eigenfrequency 5.61 Hz. The field frequency is 7.995 Hz. The pool radius $a = 0.095$ m and the depth $h = 0.113$ m; $B_0 = 0.080$ T.

unstable. In the previous section we used a linearised form of Euler's equation so the coefficient evolution equation (23) was also linear, not admitting the possibility of instability. This same equation shows that generally the expansion coefficients a_n are of first order in the expansion coefficient $\mathfrak{N}$.

To analyse non-symmetric instability it is therefore necessary to use a higher-order approximation and consider terms in Euler's equation which are quadratic in the expansion coefficients — i.e. to continue the expansion to $O(\mathfrak{N}^2)$. Again our expansion is valid for containers of arbitrary shape. Although (26) shows the $O(\mathfrak{N})$ flow to be irrotational, the $O(\mathfrak{N}^2)$ flow will not necessarily be so, but our inner product method does not necessitate an explicit calculation of this rotational flow.

3.1. Current correction

In the last section we assumed purely horizontal electric current flow, with the consequence that the boundary condition $\boldsymbol{J} \cdot \boldsymbol{n} = 0$ at the non-planar free surface $z = \eta$ is satisfied only to zeroth order. In a higher-order calculation we need to take account of the perturbation current caused by surface ripples, and also the current induced by the fluid velocity.

According to Ohm's law,

$$\boldsymbol{J} = \sigma(\boldsymbol{E} + \boldsymbol{v} \times \boldsymbol{B}). \tag{27}$$

As before we use Faraday's law to determine the electric field,

$$\boldsymbol{E} = -\omega B_0 \cos(\omega t)\nabla T \times \hat{z} + \nabla V = \boldsymbol{E}_0 + \nabla V \ \text{ say}, \tag{28}$$

where V is an arbitrary scalar potential. Substituting (28) into (27) we obtain,

$$\boldsymbol{J} = \sigma(\boldsymbol{E}_0 + \nabla V + \boldsymbol{v} \times \boldsymbol{B}) \tag{29}$$

and taking the divergence (remembering that $\boldsymbol{v}$ is irrotational to leading order) we find $\nabla^2 V = 0$. The current potential V is now uniquely determined by the boundary conditions necessary to ensure that $\boldsymbol{J}\cdot\hat{\boldsymbol{n}} = 0$ on all boundaries, namely:

$$V_z(x, y, -h) = 0, \qquad V_z(x, y, 0) = \boldsymbol{E}_0 \cdot \nabla\eta, \tag{30}$$

$$(\nabla V \cdot \hat{\boldsymbol{n}})_{S_W} = -\boldsymbol{v} \times \boldsymbol{B} \cdot \hat{\boldsymbol{n}}. \tag{31}$$

The terms ∇V and $\boldsymbol{v} \times \boldsymbol{B}$ are both $O(\mathfrak{N}\sigma E_0)$ and represent the second-order correction to the current. In GFS only the first of these terms was considered, but since they are of the same order both should be included.

A solution can be formulated by writing V as the sum of two harmonic functions $V = V_1 + V_2$. The first function is made to satisfy the free-surface condition arising from $\boldsymbol{E}_0$:

$$V_{1z}(x, y, -h) = 0, \qquad V_{1z}(x, y, \eta) = \boldsymbol{E}_0 \cdot \nabla\eta, \qquad \nabla V_1 \cdot \hat{\boldsymbol{n}} = 0 \quad \text{on } S_W; \tag{32}$$

while the second satisfies that due to the induced current:

$$V_{2z}(x, y, -h) = V_{2z}(x, y, 0) = 0, \qquad (\nabla V_2 \cdot \hat{\boldsymbol{n}})_{S_W} = -\boldsymbol{v} \times \boldsymbol{B} \cdot \hat{\boldsymbol{n}}. \tag{33}$$

We can expand V_1 in the form

$$V_1 = \omega B_0 \cos(\omega t) \sum_{n=1}^{\infty} c_n \phi_n \tag{34}$$

which immediately satisfies the first and third of conditions (32). The c_n are constant coefficients determined by the second of (32) and (28):

$$-\nabla T \times \hat{\boldsymbol{z}} \cdot \sum_{m=1}^{\infty} a_m \nabla E_m = \sum_{m=1}^{\infty} c_m E_m.$$

Multiplying each side by E_n^* and integrating over the tank cross-section, we find

$$c_n = Z_{n\alpha} a_\alpha \tag{35}$$

where the coefficient $Z_{n\alpha}$ is defined in Appendix A. In this equation, and subsequently, we use the convention that repeated Greek subscripts are summed from 1 to infinity.

The third of conditions (33) can be rewritten using (26) in the form,

$$(\nabla V_2 \cdot \hat{\boldsymbol{n}})_{S_W} = -B_0 \sin(\omega t) \dot{a}_\alpha f_\alpha(z) \frac{\partial E_\alpha}{\partial \ell},$$

where ℓ is horizontal distance around the cylinder wall. If we define a sequence of functions $\psi_n(x, y, z)$ satisfying,

$$\nabla^2 \psi_n = 0, \qquad \frac{\partial \psi_n}{\partial z}(x, y, 0) = \frac{\partial \psi_n}{\partial z}(x, y, -h) = 0,$$

$$(\nabla \psi \cdot \hat{\boldsymbol{n}})_{S_W} = f_n(z) \frac{\partial E_n}{\partial \ell}, \tag{36}$$

then the solution for V_2 can be written,

$$V_2 = -B_0 \sin(\omega t) \dot{a}_\alpha \psi_\alpha. \tag{37}$$

3.2. Euler equation and free-surface conditions

Since we neglect viscosity, fluid motion is described by Euler's equation, where now we retain terms up to $O(\mathfrak{N}^2)$. Thus the Lorentz force term now includes the currents ∇V_i and the induced current. In the quadratic acceleration term, we retain terms in v^2 where $\boldsymbol{v}$ is the $O(\mathfrak{N})$ *irrotational* velocity given by (26). Euler's equation therefore takes the form,

$$\rho \frac{\partial \boldsymbol{v}}{\partial t} + \frac{1}{2}\rho \nabla(v^2) = \frac{1}{2}\sigma\omega B_0^2 \sin(2\omega t)[\nabla T + c_\alpha \nabla\phi_\alpha \times \hat{\boldsymbol{z}}] - \sigma B_0^2 \sin^2(\omega t)[\boldsymbol{v}_H + \dot{a}_\alpha \nabla\psi_\alpha \times \hat{\boldsymbol{z}}] - \nabla P, \tag{38}$$

where $\boldsymbol{v}_H$ is the horizontal component of $\boldsymbol{v}$ and the expansion (29) has been used to express the current perturbation. In (38) the first term of the right-hand side which involves the torsion function is responsible for the forced-wave regime. The second term is a force perturbation which arises from deviation of the electric current flow due to the free surface deformation. Finally, the third and the fourth terms describe electromagnetic damping of the liquid metal flow.

On the free surface, $p = 0$, so,

$$(P)_{z=\eta} = \rho g \eta. \tag{39}$$

The kinematic boundary condition is obtained by noting that a fluid particle initially on the free surface remains there for all time. Thus

$$\frac{D}{Dt}(z-\eta) = v_z - \frac{\partial \eta}{\partial t} - \boldsymbol{v}\cdot\nabla\eta = 0.$$

Differentiating with respect to time we obtain

$$\dot{v}_z - \dot{\boldsymbol{v}}\cdot\nabla\eta = \ddot{\eta} + \boldsymbol{v}\cdot\nabla\dot{\eta}. \tag{40}$$

3.3. Evolution equation

As before, the evolution equation is obtained by taking the inner product of (38) with the $\nabla\phi_n^*$.

Term 1. For the first term we find

$$I_1 = \rho\langle\dot{\boldsymbol{v}}, \nabla\phi_n\rangle = \int_V \nabla\cdot(\phi_n^*\dot{\boldsymbol{v}})\,\mathrm{d}V = \rho\int_{S_F}\phi_n^*\dot{\boldsymbol{v}}\cdot\mathbf{dS},$$

where S_F is the free surface $z = \eta$, the tank walls and base giving no contribution to the surface integral. The surface element on F is given by

$$\mathbf{dS} = (\hat{z} - \nabla\eta)\,\mathrm{d}x\,\mathrm{d}y$$

so we can use (40) to obtain

$$I_1 = \rho\int_F \phi_n^*(x, y, \eta)(\ddot{\eta} + \boldsymbol{v}\cdot\nabla\dot{\eta})\,\mathrm{d}x\,\mathrm{d}y. \tag{41}$$

To evaluate ϕ_n^* on the free surface $z = \eta$ we expand as a Taylor series about $z = 0$ using (18) and (19), and find that the first term of (41) gives

$$\int (s_n + \eta)E_n^*\ddot{\eta}\,\mathrm{d}x\,\mathrm{d}y, \quad s_n = f_n(0) = \frac{1}{T_n\lambda_n}.$$

Using the expansion (15) and the orthogonality of the eigenfunctions this can be written

$$\|E_n\|^2(s_n\ddot{a}_n + Q_{n\alpha\beta}a_\alpha\ddot{a}_\beta) \quad \text{(summation convention)}, \tag{42}$$

where the coefficient $Q_{n\alpha\beta}$ is defined in Appendix A. The second term of (41) is quadratic in the coefficients a_n so to order $\mathfrak{N}^4$ we simply integrate over the unperturbed free surface $z = 0$. Using similar methods we obtain the expression

$$\|E_n\|^2 s_n s_\alpha Q'_{n\alpha\beta}\dot{a}_\alpha\dot{a}_\beta \tag{43}$$

(see Appendix A). Combining (42) and (43) we find

$$I_1 = \rho\|E_n\|^2[s_n\ddot{a}_n + Q_{n\alpha\beta}a_\alpha\,\ddot{a}_\beta + s_n s_\alpha Q'_{n\alpha\beta}\dot{a}_\alpha\dot{a}_\beta]. \tag{44}$$

To leading order in $\mathfrak{N}$ we may replace $\ddot{a}_\beta$ in the quadratic term of (44) by

$$\ddot{a}_\beta = -\Omega_\beta^2 a_\beta,$$

maintaining the same level of approximation.

Term 2. The inner product arising from term 2 is,

$$\left\langle\frac{1}{2}\nabla(v^2), \nabla\phi_n\right\rangle = \frac{1}{2}\int_V \nabla\cdot(v^2\nabla\phi_n^*)\,\mathrm{d}V = \frac{1}{2}\int_F v^2 E_n^*\,\mathrm{d}x\,\mathrm{d}y. \tag{45}$$

Since this expression is quadratic in v and terms of order $\mathfrak{N}^4$ or higher are neglected, we may take the free surface to be $z = 0$. Likewise we use (26) for the velocity field and find

$$(v^2)_{z=0} = s_\alpha s_\beta[\nabla E_\alpha\cdot\nabla E_\beta + E_\alpha E_\beta]\dot{a}_\alpha\dot{a}_\beta,$$

then substitute into (45) to obtain,

$$I_2 = \frac{1}{2}\rho \|E_n\|^2 [s_\alpha s_\beta Q'_{n\alpha\beta} + Q_{n\alpha\beta}]\dot{a}_\alpha \dot{a}_\beta. \tag{46}$$

Term 3. Taking the inner product of $\nabla\phi_n$ with the first term on the right-hand side of (38) we first note that since T is independent of z,

$$\int_V \nabla T \cdot \nabla \phi_n^* \,\mathrm{d}V = \int_{-h}^{\eta} \mathrm{d}z \int f_n(z) \nabla T \cdot \nabla E_n^* \,\mathrm{d}x\,\mathrm{d}y.$$

The result of the z-integration is $\lambda_n^{-2} + \eta s_n + \mathrm{O}(\mathfrak{N}^4)$, and the integral reduces to,

$$\|E_n\|^2 (\Gamma_n + s_n R_{n\alpha} a_\alpha). \tag{47}$$

The remaining contribution to term 3 is

$$\int_V c_\alpha (\nabla\phi_\alpha \times \hat{z}) \cdot \nabla \phi_n^* \,\mathrm{d}x\,\mathrm{d}y\,\mathrm{d}z = c_\alpha F_{n\alpha} S_{n\alpha}, \tag{48}$$

(see Appendix A). Using (35) we can combine (47) and (48) and write

$$I_3 = \frac{1}{2}\sigma\omega B_0^2 \sin(2\omega t)\big[\Gamma_n \|E_n\|^2 + \big(\|E_n\|^2 s_n R_{n\alpha} + Z_{\alpha\beta} S_{n\beta} F_{n\beta}\big) a_\alpha\big]. \tag{49}$$

In the right-hand side of (49) the term involving Γ_n corresponds to the forcing of the axisymmetric modes. It vanishes for the non-symmetric modes ($m \neq 0$).

Term 4. The inner product $\langle \nabla\psi_\alpha \times \hat{z}, \nabla\phi_n \rangle$, can be written in terms of the coefficients defined in Appendix A, as

$$s_n \|E_n\|^2 T_{n\alpha}. \tag{50}$$

Also,

$$(\boldsymbol{v} \times \hat{z}) \times \hat{z} = \boldsymbol{v} - v_z \hat{z} = \dot{a}_\alpha f_\alpha(z) \nabla E_\alpha,$$

so taking the inner product with $\nabla\phi_n$ and using (17) yields,

$$F_{nn} \dot{a}_n \lambda_n^2 \|E_n\|^2.$$

Thus the complete inner product from term 4 is,

$$I_4 = -\sigma\omega B_0^2 \sin^2(\omega t)[s_n T_{n\alpha} \dot{a}_\alpha + F_{nn} \lambda_n^2 \dot{a}_n] \|E_n\|^2. \tag{51}$$

Term 5. The final inner product

$$I_5 = \langle \nabla P, \nabla\phi_n \rangle = \int_V \nabla \cdot (P \nabla \phi_n^*) \,\mathrm{d}V = \int_F \rho g \eta \nabla \phi_n^* \cdot (\hat{z} - \nabla\eta) \,\mathrm{d}x\,\mathrm{d}y,$$

using (39). Arguments similar to those already used show that

$$I_5 = \rho g a_n \|E_n\|^2 + \frac{1}{2}\rho g \|E_n\|^2 s_n \lambda_n^2 Q_{n\alpha\beta}\, a_\alpha a_\beta. \tag{52}$$

Collecting terms I_1 to I_5 we obtain the evolution equation,

$$\begin{aligned} &\ddot{a}_n + \mathfrak{N}\omega\nu_n \sin^2(\omega t)\dot{a}_n + \Omega_n^2 (a_n + U_{n\alpha\beta} a_\alpha a_\beta) + V_{n\alpha\beta} \dot{a}_\alpha \dot{a}_\beta \\ &\quad = \frac{1}{2}\omega^2 \mathfrak{N} \sin(2\omega t)(\lambda_n T_n + W_{n\alpha} a_\alpha) - \omega \mathfrak{N} \sin^2(\omega t) T_{n\alpha} \dot{a}_\alpha, \end{aligned} \tag{53}$$

where the coefficients ν_n, $U_{n\alpha\beta}$, $V_{n\alpha\beta}$, $W_{n\alpha}$ and $T_{n\alpha}$ are defined in Appendix A. Note that if we discard $\mathrm{O}(\mathfrak{N}^2)$ terms from this equation — remembering that the a_n coefficients are $\mathrm{O}(\mathfrak{N})$ — we recover (23).

3.4. Growth of a non-axisymmetric mode in a circular or annular tank

We can use (53) to derive an equation for the growth of non-symmetric modes. Suppose that all non-symmetric modes are of small amplitude, say ϵ where $\epsilon \ll \mathfrak{N}$. In (53) we let a_n be a non-symmetric mode with azimuthal wavenumber m, and neglect terms of $O(\epsilon^2)$. The U and V terms which involve double summations require special care. Since we neglect $O(\epsilon^2)$ terms in

$$U_{n\alpha\beta}a_\alpha a_\beta$$

either a_α or a_β must represent a symmetric mode with coefficient $\mathfrak{N}\sin(2\omega t)h_\alpha$ or $\mathfrak{N}\sin(2\omega t)h_\beta$ (24). The U term can therefore be written in the form,

$$\mathfrak{N}\sin(2\omega t)(U_{n\alpha\beta} + U_{n\beta\alpha})h_\alpha a_\beta. \tag{54}$$

Moreover, $U_{n\alpha\beta}$ is proportional to the coefficient

$$Q_{n\alpha\beta} = \|E_n\|^{-2}\int_{S_0} E_n^* E_\alpha E_\beta \,\mathrm{d}x\,\mathrm{d}y,$$

(A.1). Since the azimuthal wavenumbers for E_α and E_n and 0 are m respectively, the Q coefficient vanishes unless E_β, and hence a_β also represent waves of azimuthal wavenumber m. Thus in (54) the a_α are all of azimuthal wavenumber m, and the evolution equation for a_n involves *only coefficients of the same azimuthal wavenumber*. In other words the non-symmetric modes for various m evolve *independently*. The V term can be dealt with similarly, and the evolution equation takes the form,

$$\begin{aligned}&\ddot{a}_n + \mathfrak{N}\omega v_n \sin^2(\omega t)\dot{a}_n + \Omega_n^2\big[a_n + \mathfrak{N}\sin(2\omega t)u_{n\alpha}a_\alpha\big] + 2\mathfrak{N}\omega\cos(2\omega t)v_{n\alpha}\dot{a}_\alpha\\ &\quad= \frac{1}{2}\omega^2\mathfrak{N}\sin(2\omega t)W_{n\alpha}a_\alpha - \omega\mathfrak{N}\sin^2(\omega t)T_{n\alpha}\dot{a}_\alpha, \quad n = 1, 2, 3, \ldots,\end{aligned} \tag{55}$$

where the coefficients $u_{n\alpha\beta}$, $v_{n\alpha\beta}$ are defined in Appendix A.

In (55) the two coefficients of $\sin^2(\omega t)$ represent electromagnetic damping. The first term of the right-hand side includes the destabilising force perturbation derived by GFS. The terms $u_{n\alpha}$, $v_{n\alpha}$ represent nonlinear interaction with symmetric modes and may be also destabilizing, depending on the value of the magnetic field frequency as we shall see later.

4. Results and comparison with experiments

4.1. Onset of parametric instability

Eqs. (55) are linear with periodic coefficients — essentially a system of coupled Mathieu–Hill equations. Providing the interaction coefficient $\mathfrak{N}$ is small, there are simple approximate criteria for the onset of parametric instability [8]. These can be expressed in terms of the various equation coefficients, formulae for which in the case of the circular cylinder are given in Appendix B. Certain of the coefficients such as the $Q_{n\alpha\beta}$ cannot be expressed by a simple formula, and must be found by numerical integration. The corresponding coefficients for the narrow-gap annulus are given in Appendix C, and illustrate how pool geometry may select the type of transition. Experiments have been performed in an annular tank [9].

Whether a solution of (55) grows or decays depends on the values of the interaction parameter $\mathfrak{N}$ and the forcing frequency 2ω. Regions of instability may arise from points on the $\mathfrak{N} = 0$ axis in the $(\omega, \mathfrak{N})$-plane where the natural frequencies are simply related to the forcing frequency. Specifically such *resonance points* occur when,

$$\omega = \Omega_n, \quad \omega = \frac{\Omega_n + \Omega_m}{2}, \quad \text{or} \quad \omega = \frac{\Omega_n - \Omega_m}{2}.$$

We refer to these as type I, type II and type III resonances respectively. The approximate theory [8] gives simple criteria for determining whether or not a particular resonance point is the source of an instability region. Stability depends essentially on the relative strengths of the damping and forcing terms. When an instability region does arise it is bounded by a pair of straight lines of equal and opposite slope passing through the resonance point. The earlier paper GFS did not include electromagnetic damping and all resonance points generated instability regions, but we shall see that many of these disappear when damping is included.

The approximate theory [8] shows that instability at a resonance point can be analysed with a reduced set of Eqs. (55) consisting of only those equations involving the natural frequencies Ω_n, Ω_m which determine the resonance point. Thus for a type I resonance we need consider only a single equation, and for type II and type III resonances a pair of equations.

There is however another important factor. It can be seen from (25) or (B.2) that the axisymmetric coefficients h_n become very large when

$$\Omega_n^2 \approx 4\omega^2.$$

Thus, when $\omega \approx \frac{1}{2}\Omega_n$ the coefficients $u_{n\alpha}$, $v_{n\alpha}$ in (55) also become large. We have in effect a "dual resonance" between axisymmetric and non-axisymmetric modes. In the simple $\mathfrak{N} \ll 1$ theory it is assumed that ω is constant but clearly, because of the possibility of axisymmetric mode resonance, variations in ω must have an important effect. The simple approximate theory does not give an accurate global picture of the stability boundaries.

To compare theory and experiment the stability boundaries were therefore calculated numerically. To determine the stability of a point in the $(\omega, \mathfrak{N})$-plane, the Floquet matrix was calculated by numerical integration of (55). The eigenvalues were then calculated numerically, an eigenvalue with absolute value greater than unity indicating instability. The stability boundary search was started at a resonance point $\omega = \Omega_n$ on the ω-axis, then tracked by finding two further points on either side of the boundary and locating the next boundary point by a bisection method.

4.2. The circular cylinder

The paper GFS made a comparison between the theoretical and observed critical magnetic field strength necessary to excite various parametric instabilities. The agreement was only qualitatively correct and the more complete analysis given here might be expected to give better results.

We should however point out that comparison with experiment is fraught with difficulty, and we cannot expect exact quantitative agreement. The critical value of $\mathfrak{N}$ necessary to excite an instability, say $\mathfrak{N}_C$ is very sensitive to the frequency, and a small error in f may produce a large relative error in $\mathfrak{N}_C$. Also a small difference between the experimental eigenfrequencies and the theoretical ones may produce a relatively large change in the theoretical value of $\mathfrak{N}_C$. The theoretical determination (23) of the eigenfrequencies may become inaccurate for small wavelengths because of the complex dynamics of the meniscus near the lateral wall [10]. Indeed, in calculating natural frequencies we have used the meniscus correction suggested in this paper. Although we have included electromagnetic damping, other damping sources have been neglected, such as viscosity and, perhaps more importantly, damping due to movement of the mercury meniscus on the tank walls. The latter effect would be difficult to calculate theoretically, but a method has been suggested by Hocking [11]. Meniscus damping was considered by Ursell [12] to be the main source of disagreement between theory and experiment. We therefore expect theoretical predictions of $\mathfrak{N}_C$ to be somewhat smaller than experimentally measured values.

The approximate theory for type I resonances show that for $m \leqslant 7$ only the basic $n = 1$ mode with eigenfunction $J_m(\lambda_{m1})$ gives rise to a parametric instability in the range of experimental frequencies used by Galpin and Fautrelle [1]. It appears that electromagnetic damping eliminates the $n > 1$ modes of shorter radial wavelength. For $m > 7$, type I resonances occur for all n in the range 1–10 (at least), but the $n = 1$ mode always has by far the largest growth rate. Indeed only $n = 1$ modes have been observed experimentally. All type II resonances appear to be destabilising, but the lowest frequency is about 8.5 Hz, at the upper end of the experimental range. None of the first 60 type III resonances is destabilising. Note that the type I instability is created by the interaction with the axisymmetric modes as well as the perturbation of the basic electric current as discussed by Galpin et al. [2].

Table 1
Experimental results of Galpin [13] and Galpin and Fautrelle [1] obtained in a mercury cylindrical tank with $a = 0.095$ m and depth $h = 0.113$ m. The m column lists the azimuthal wave number; F^m and F_c^m denote respectively the values of the eigenfrequencies given by the simple formula (23) and the corrected estimates given by Miles [10]. $\mathfrak{N}$ is the experimentally observed stability threshold and $\mathfrak{N}'$ the theoretically calculated threshold. Frequencies are given in Hz

(m)	F^m	F_c^m	f	$\mathfrak{N}$	$\mathfrak{N}'$
3	3.315	3.321	3.37	0.114	0.097
4	3.730	3.743	3.63	0.208	0.116
4	3.730	3.743	3.78	0.093	0.043
4	3.730	3.743	3.84	0.161	0.151
5	4.097	4.120	4.03	0.138	0.077
6	4.430	4.467	4.43	0.106	0.026
8	5.023	5.100	5.05	0.051	0.012
11	5.792	5.954	6.00	0.044	0.035
15	6.672	7.010	7.00	0.026	0.026

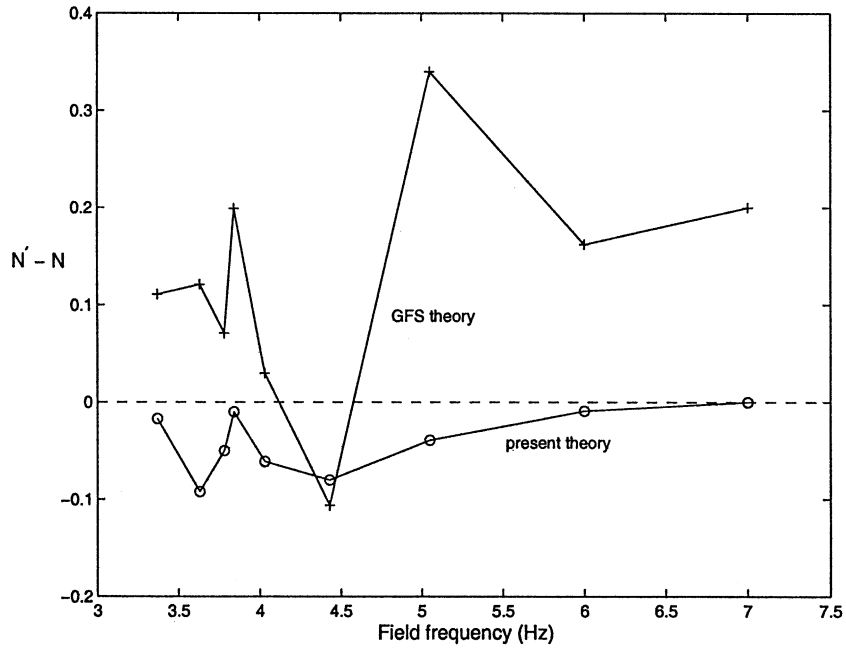

Fig. 4. Comparison between theory and experiment. The points marked with circles show to the difference between the experimental value of $\mathfrak{N}_c$ and that derived from the present theory. The crosses show differences based on the GFS theory. The pool radius $a = 0.095$ m and the depth $h = 0.113$ m.

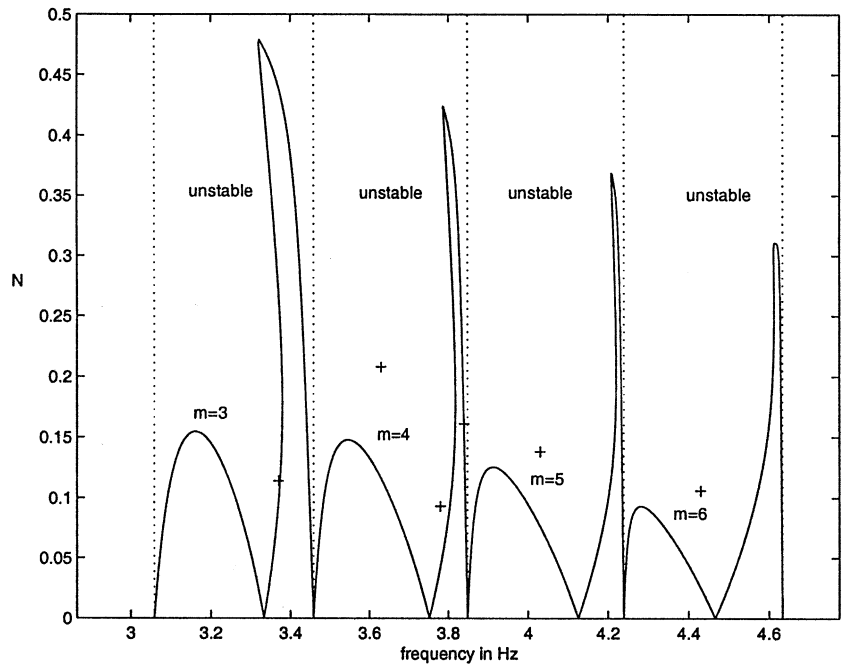

Fig. 5. Stability boundaries for modes $m = 3$ to $m = 6$.

The experiments described by Galpin and Fautrelle [1] and by Galpin [13] included only a few measurements of $\mathfrak{N}_C$, all made in the vicinity of type I resonances. Table 1 summarises the results. The values of the eigenfrequencies F^m correspond to the simple formula (23). However, to achieve the comparison we use a corrected estimate F_c^m established by Miles [10]. That correction takes into account both surface tension and the meniscus effects near the pool edge.

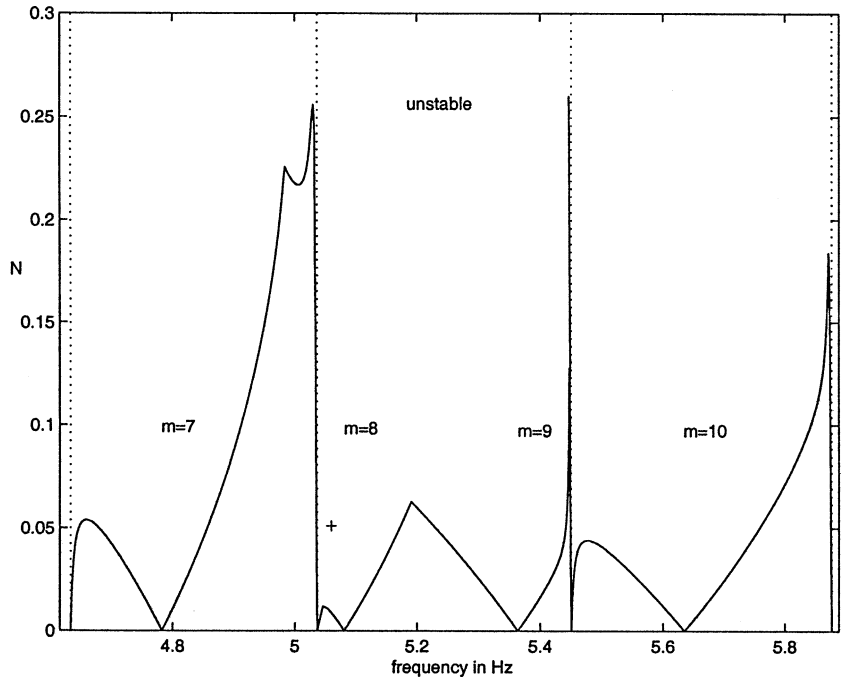

Fig. 6. Stability boundaries for modes $m = 7$ to $m = 10$.

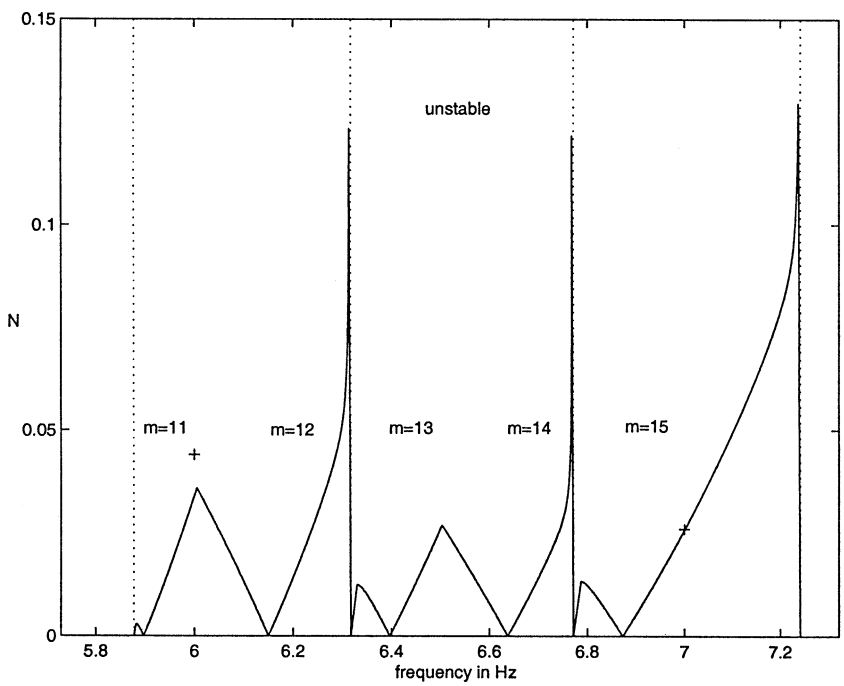

Fig. 7. Stability boundaries for modes $m = 11$ to $m = 15$.

The agreement between the observed and calculated stability threshold is erratic, but as expected, the theoretical value $\mathfrak{N}'$ is always smaller than the observed value $\mathfrak{N}$. Some of the difference may therefore be attributed to neglected sources of damping. Fig. 4 illustrates the difference between the GFS calculations of $\mathfrak{N}_C$ and the present results. Generally the GFS predictions

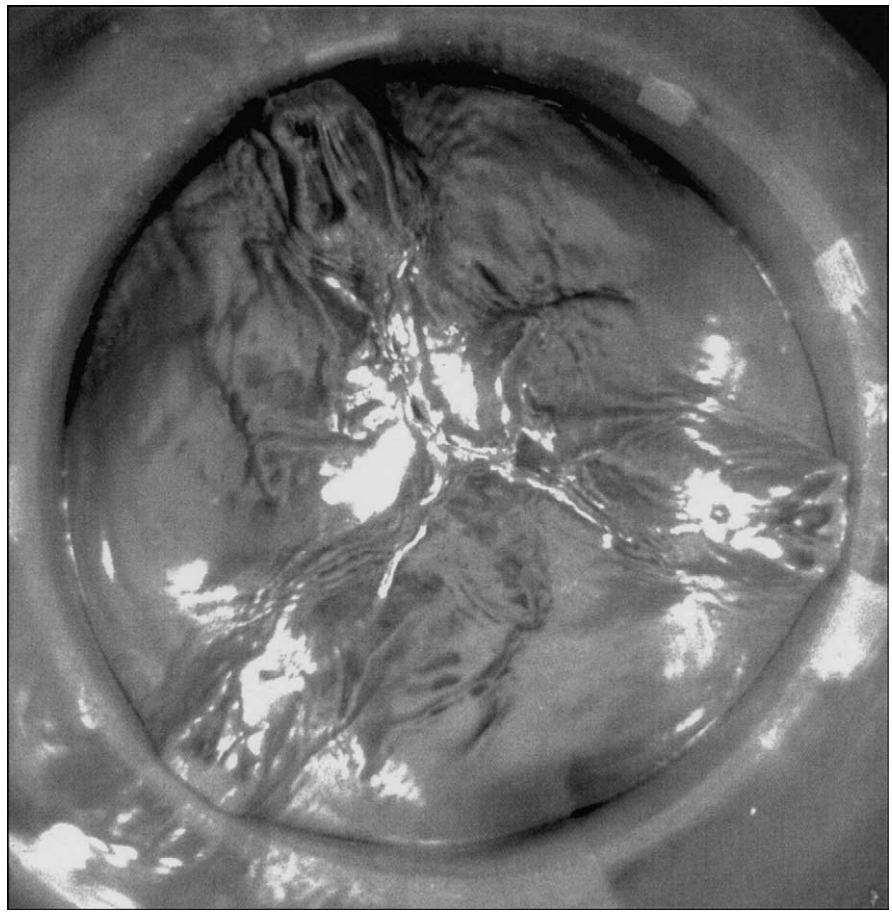

Fig. 8. Pattern corresponding to a sub-harmonic regime (type I) observed on the free surface of a cylindrical mercury pool. The observed dominant mode is (3,1) with eigenfrequency 3.43 Hz. The applied frequency is 3.20 Hz, $a = 0.095$ m, $h = 0.113$ m, $B_0 = 0.28$ T.

are too high, probably because nonlinear mode interactions were neglected. The present theory is also much more accurate at higher frequencies.

Figs. 5–7 show numerically-calculated stability boundaries over the range 2.8 Hz to 7.3 Hz. The points in the $(\omega, \mathfrak{N})$-plane at which transition to instability has been observed are marked by crosses, and it can be seen that these are generally close to the boundaries. The dotted vertical lines mark resonant frequencies of axisymmetric modes. The stability boundary approaches the $\mathfrak{N} = 0$ axis in the vicinity of these lines, indicating strong destabilisation by large-amplitude axisymmetric modes. The natural frequency correction due to Miles [10] was used throughout.

Fig. 8 shows some typical type I resonances in a cylindrical mercury tank of radius 9.5 cm. In both cases the forced waves are always superimposed on the azimuthal modes. Accordingly, identification from a photograph is not so easy. However, analysis of the video as well as the instantaneous amplitude recordings allow the identification of the resonance type [1]. In Fig. 8 for example, the dominant mode is (3,1) whose eigenfrequency is close to the magnetic field frequency.

4.3. The narrow annulus

Experiments have been performed in annular tanks $a \leqslant r \leqslant b$ by Fautrelle [9]. If we assume a narrow gap, taking $(b-a) \ll a$ the analysis is greatly simplified, and the coefficients can all be expressed by simple formulae given in Appendix C. It is noteworthy that the matrices $u_{n\alpha}$, $v_{n\alpha}$ and $W_{n\alpha}$ have zero coefficients on their diagonal. Sneyd [8] has shown that in that case only type II resonances occur.

A numerical calculation of the stability boundary is shown in Fig. 9. For consistency with the assumptions, only small values of $\mathfrak{N}$ may be considered. Two non-symmetric modes have been considered, namely a_0 and a_1 for $m = 3$ corresponding to experiments discussed below. The results confirm that only the type II, i.e., the combination resonance appears. Note that

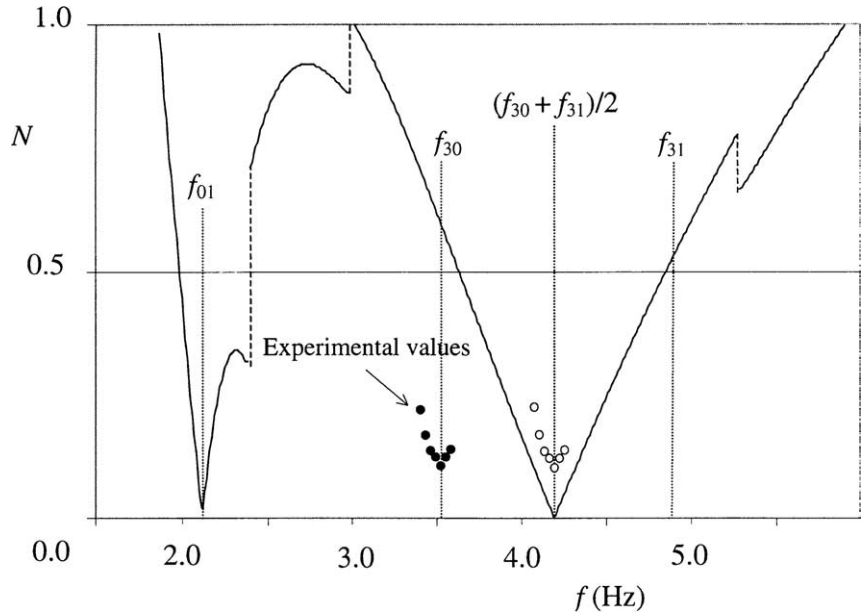

Fig. 9. Computed stability diagram for a narrow mercury annulus, using two-mode truncation. The critical value of the interaction parameter $\mathfrak{N}$ is plotted versus the field frequency in Hz. The eigenfrequencies of the modes (3,0) and (3,1) are $f_{3,0} = 3.526$ Hz and $f_{3,1} = 4.862$ Hz respectively in the narrow gap approximation. In the annulus case with finite gap, the theoretical eigenfrequencies of the modes (3,0) and (3,1) are $f'_{3,0} = 2.558$ Hz and $f'_{3,1} = 4.422$ Hz respectively. The dots represent experimental points. The circles correspond to the experimental values which have been shifted to coincide with the values of the narrow-gap approximation.

there also exists a strong resonance for $f = 2.12$ Hz. Actually, the latter frequency corresponds to a resonance point for the first axisymmetric mode, so the coefficient h_1 in (24) becomes large. Accordingly, the coefficients of the matrices $u_{n\alpha}$, $v_{n\alpha}$ become large as well, and the stability of the system is lowered. The latter result confirms that forced mode may also indirectly destabilise the system.

Another series of experiments was performed in an annular tank $a \leqslant r \leqslant b$ by Debray and Fautrelle [9] and Debray [14]. Here the inner tank radius was 5 cm and the outer 9 cm, so the narrow-gap approximation caused some inaccuracy. However this approximation is probably adequate for estimating the coefficients, given the other sources of experimental error. Two main discrepancies arise from the use of the narrow gap approximation. First, the natural frequencies are different, although the orders of magnitude are similar. Second, the experimental geometry in Debray and Fautrelle [9] is intermediate between the circular cylinder and the narrow annulus, so that in the experiments both type I and type II resonances are observed. However, the experiments indicate that the strongest resonances correspond to type II transitions.

For example a type II resonance involving the modes (3,0) and (3,1) ($m = 3$) was observed and analysed. The results are illustrated in Fig. 9. The experimental stability boundary is shown and compared with the results of the narrow gap theory. Note that in those experiments the mercury was covered by a water layer of 0.10 m depth. It was checked that in the experiment the stability "tongue" was a mode combination transition involving the modes (3,0) and (3,1) with eigenfrequencies $f'_{3,0} = 2.56$ Hz and $f'_{3,1} = 4.42$ Hz respectively. Those eigenfrequencies were very close to the theoretical estimates taking into account both surface tension and the presence of the water layer for a finite gap annulus. The present theoretical stability boundary is shifted because of the narrow gap approximation which yields different values of the eigenfrequencies. However, the slopes of the theoretical and experimental stability boundaries are quite similar. The theoretical threshold is consistently lower than the experimental one, as expected.

Fig. 10 shows a typical type II resonance in an annulus Debray and Fautrelle [9]. The dominant modes are (3,0) and (3,1).

5. Discussion and conclusions

We have considered the effects of a very low frequency A.C. magnetic field on a liquid metal domain having a free surface. The analysis is based on an inner product method, and various shapes of liquid domain have been considered. We show that the magnetic field has two major effects. First, it creates forced standing surface waves. These forced waves possess the same symmetry properties as the liquid domain. It is noteworthy that they may be described by a simple torsion function which

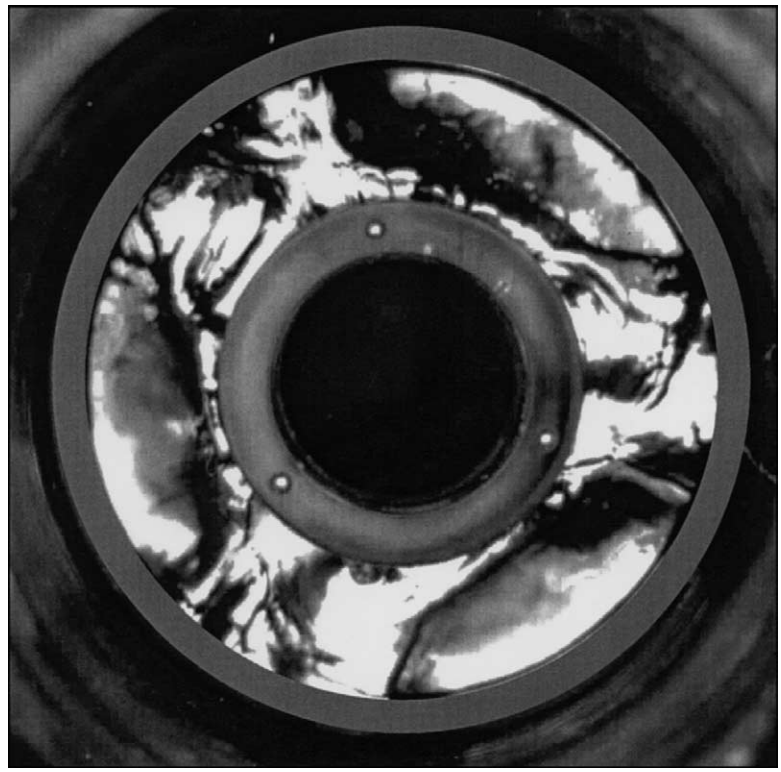

Fig. 10. View of a type II regime in a mercury annulus Debray and Fautrelle [9] without a covering water layer. The dominant modes are (3,0) and (3,1), whose theoretical eigenfrequencies respectively are 2.76 Hz and 4.76 Hz. The frequency and strength of the magnetic field respectively are 3.86 Hz and 0.23 T. The pool dimensions are $a = 5$ cm, $b = 9$ cm and $h = 2$ cm.

can be easily determined for many domain shapes. Second, it is shown that non-symmetric modes may be unstable when the magnetic field amplitude exceeds a critical value. This instability may appear as a simple parametric resonance (the so-called type I resonance) or as combined-mode resonances (type II or type III resonances). The appearance of type I and II transitions have been confirmed by experiments in annular tanks.

This instability originates from two main mechanisms. First, the non-symmetric free-surface displacements create perturbations of the basic (symmetric) electric current, which lead to destabilising electromagnetic force perturbations. Second, nonlinear interaction with the forced symmetric solution is also destabilising. Note that in the circular cylinder case, the latter mechanism is predominant. It is also found that the shape of the tank influences the transition type. For example, in the narrow annulus case only mode-combination instability may be obtained, whilst in the circular cylinder both type I and type II transitions are observed.

The solution procedure is facilitated by the fact that the $O(\mathfrak{N})$ forced waves are irrotational, and that the inner product method makes a detailed calculation of the $O(\mathfrak{N}^2)$ rotational flow unnecessary. Note that in the experiments Galpin [13] the surface wave pattern was very stable and could be observed for several thousands of oscillation periods. Some rotational motions have been observed only for a magnetic field frequency greater than approximately 10 Hz.

From the comparison between the theoretical and experimental results we see that experimental magnetic field thresholds are greater than the theoretical ones. One reason could be viscous damping which is not taken into account in the present theory. In particular, two types of viscous boundary layer will form on the tank walls. First, we may find boundary layers generated by the external oscillatory flow, whose thickness is Batchelor [6]

$$O\left(\frac{\nu^{1/2}}{\omega}\right).$$

For mercury and a magnetic field frequency $f = 2$ Hz, the typical depth of the viscous layer is 90 μm. Second, the viscous layers may be of Hartmann type. Consider for example the boundary perpendicular to the magnetic field — i.e. on the tank base.

Eq. (38) may be considered as a core flow equation, and the wall no-slip condition is achieved through an (unsteady) Hartmann layer, whose thickness is

$$\mathrm{O}\left(\frac{\rho\nu}{\sigma B_0^2}\right)^{1/2}.$$

Taking $B_0 = 0.2$ T yields a value of 184 μm. The depths of these two layers are comparable and quite small, so we might expect significant wall friction, which could partly explain the discrepancy between theory and experiment.

The case of the rectangular tank has not been investigated in detail. Although the geometry is quite simple and the torsion function can be readily calculated, it does not possess such a high degree of symmetry as the cylinder or annulus. Thus, the nonlinear interaction are more complex, and further investigation is needed.

Appendix A. Coefficient definitions

A.1. Basic coefficients

$$\begin{aligned}
&T_n = \tanh(\lambda_n h), \qquad s_n = \frac{1}{T_n\lambda_n}, \qquad \Omega_n^2 = \frac{g}{s_n},\\
&\Gamma_n = \|E_n\|^{-2}\int_{S_0} T E_n^*\,\mathrm{d}x\,\mathrm{d}y, \qquad h_n = \frac{\lambda_n\Gamma_n T_n}{8[(\Omega_n^2/4\omega^2)-1]},\\
&Q_{npq} = \|E_n\|^{-2}\int_{S_0} E_n^* E_p E_q\,\mathrm{d}x\,\mathrm{d}y,\\
&Q'_{npq} = \|E_n\|^{-2}\int_{S_0} E_n^*\nabla E_p\cdot\nabla E_q\,\mathrm{d}x\,\mathrm{d}y = \frac{1}{2}Q_{npq}\left(\lambda_p^2+\lambda_q^2-\lambda_n^2\right)
\end{aligned} \tag{A.1}$$

(see Appendix D).

$$R_{np} = \|E_n\|^{-2}\int_{S_0}(\nabla T\cdot\nabla E_n^*)E_p\,\mathrm{d}x\,\mathrm{d}y$$

on Pattern corresponding to a sub-harmonic regime (type I) observe

$$S_{np} = \int_C E_n^*\nabla E_p\cdot\mathbf{dl}, \qquad Z_{n\alpha} = \|E_n\|^{-2}\int_{S_0} E_n^*[T,E_\alpha]\,\mathrm{d}x\,\mathrm{d}y,$$

$$T_{np} = -s_n^{-1}\|E_n\|^{-2}\int_{S_W} f_n(z)\psi_p\frac{\partial E_n^*}{\partial\ell}\,\mathrm{d}S, \qquad F_{pq} = \int_{-h}^{0} f_p(z)f_q(z)\,\mathrm{d}z.$$

The integral F_{pq} can be evaluated by elementary methods:

$$F_{pq} = \frac{s_p - s_q}{\lambda_q^2-\lambda_p^2} \quad (p\neq q), \qquad F_{pp} = \frac{2\lambda_p h + \sinh(2\lambda_p h)}{4\lambda_p^3\sinh^2(\lambda_p h)}.$$

Note that $[f,g]$ denotes the Jacobian of the functions f and g.

A.2. Evolution equation coefficients

$$
\begin{aligned}
&\nu_n = \frac{F_{nn}\lambda_n^2}{s_n}, \qquad V_{n\alpha\beta} = s_\alpha\left(1+\frac{s_\beta}{2s_n}\right)Q'_{n\alpha\beta} + \frac{1}{2s_n}Q_{n\alpha\beta},\\
&W_{np} = R_{np} + \frac{Z_{p\beta}S_{n\beta}F_{n\beta}}{\|E_n\|^2 s_n}, \qquad U_{n\alpha\beta} = \left[\frac{s_n\lambda_n^2}{2} - \frac{1}{s_\beta}\right]Q_{n\alpha\beta},\\
&\overline{U}_{n\alpha\beta} = U_{n\alpha\beta} + U_{n\beta\alpha} = \left[s_n\lambda_n^2 - \frac{1}{s_\alpha} - \frac{1}{s_\beta}\right]Q_{n\alpha\beta},\\
&\overline{V}_{n\alpha\beta} = V_{n\alpha\beta} + V_{n\beta\alpha} = Q'_{n\alpha\beta}\left(s_\alpha + s_\beta + \frac{s_\alpha s_\beta}{s_n}\right) + \frac{1}{s_n}Q_{n\alpha\beta},\\
&u_{n\alpha} = \overline{U}_{n\alpha\beta}h_\beta, \qquad v_{n\alpha} = \overline{V}_{n\alpha\beta}h_\beta.
\end{aligned}
\tag{A.2}
$$

Appendix B. Coefficients for the circular cylinder

Note firstly that

$$
\|E_n^m\|^2 = 2\pi\int_0^a J_m^2(\lambda_{mn}r)r\,\mathrm{d}r = \frac{\pi}{\lambda_{mn}^2}\left[\lambda_{mn}^2a^2 - m^2\right]J_m^2(\lambda_{mn}a), \tag{B.1}
$$

$$
h_n = \frac{T_n}{8\lambda_{0n}J_0(\lambda_{0n}a)[1-(\Omega_n^2/4\omega^2)]}. \tag{B.2}
$$

The T_{np} coefficients: The ψ functions are given by,

$$
\psi_n^m = \frac{\mathrm{i}r^m}{ha^m\lambda_{mn}^2}J_m(\lambda_{mn}a)\,\mathrm{e}^{\mathrm{i}m\theta} + \frac{2\mathrm{i}mJ_m(\lambda_{mn}a)}{ah}\sum_{k=1}^{\infty}\frac{I_m(\mu_k r)\cos(\mu_k z)}{\mu_k(\mu_k^2+\lambda_{mn}^2)I'_m(\mu_k a)}\,\mathrm{e}^{\mathrm{i}m\theta}, \tag{B.3}
$$

where $\mu_k = k\pi/h$. Using this formula we obtain,

$$
\begin{aligned}
s_n^m\|E_n^m\|^2T_{np} = {}& \frac{-2\pi m}{h\lambda_{mn}^2\lambda_{mp}^2}J_m(\lambda_{mn}a)J_m(\lambda_{mp}a)\\
&- \frac{4\pi m^2}{ah}J_m(\lambda_{mn}a)J_m(\lambda_{mp}a)\sum_{k=1}^{\infty}\frac{I_m(\mu_k a)}{I'_m(\mu_k a)\mu_k(\mu_k^2+\lambda_{mn}^2)(\mu_k^2+\lambda_{mp}^2)}.
\end{aligned}
$$

The R_{np} coefficient:

$$
R_{np} = \frac{\pi\lambda_{mn}}{\|E_n^m\|^2}\int_0^a r^2J_{m+1}(\lambda_{mn}a)J_m(\lambda_{mp}a)\,\mathrm{d}r - \frac{1}{2}m\delta_m^p.
$$

The W_{np} coefficient: First we calculate

$$
S_{np} = \int_C \left(E_n^m\right)^*\nabla E_p^m\cdot\mathbf{dl}.
$$

Expanding,

$$
S_{np} = 2\pi\,\mathrm{i}mJ_m(\lambda_{mn}a)J_m(\lambda_{mp}a).
$$

Next:

$$
\|E_n^m\|^2Z_{np} = \int_S \left(E_n^m\right)^*\left[T, E_p^m\right]\mathrm{d}x\,\mathrm{d}y = \int_S \left(E_n^m\right)^*\frac{\partial(E_p^m, T)}{\partial(r,\theta)}\,\mathrm{d}r\,\mathrm{d}\theta,
$$

$$\int_S \left(E_n^m\right)^* \frac{\partial E_p^m}{\partial \theta}\frac{\partial T}{\partial r}\,\mathrm{d}r\,\mathrm{d}\theta = -\pi \mathrm{i}m \int r J_m(\lambda_{mn} r) J_m(\lambda_{mp} r)\,\mathrm{d}r.$$

$$Z_{np} = -\frac{1}{2}\mathrm{i}m\delta_{np}$$

in view of the orthogonality of the Bessel functions. It now follows that

$$W_{np} - R_{np} = \frac{Z_{p\beta} S_{n\beta} F_{n\beta}}{\|E_n\|^2 s_n} = \pi m^2 \delta_{p\beta} \frac{J_m(\lambda_{mn} a) J_m(\lambda_{m\beta} a) F_{n\beta}}{s_n \|E_n\|^2}$$
$$= \pi m^2 \frac{J_m(\lambda_{mn} a) J_m(\lambda_{mp} a) F_{np}}{s_n \|E_n\|^2} = \frac{\lambda_n^2 m^2}{s_n(\lambda_n^2 a^2 - m^2)} \left(\frac{J_m(\lambda_{mp} a)}{J_m(\lambda_{mn} a)}\right) F_{np}.$$

B.1. Comparison with GFS (1992)

A useful check is to compare this term with the C_{np} in GFS (1992). Given that

$$\alpha_n \text{ (GFS)} = \frac{a_n J_m(\lambda_{mn} a)}{a} \text{ (present paper)},$$

we should find that

$$\Omega_n^2 L_0 C_{n\alpha} \left(\frac{J_m(\lambda_{m\alpha} a)}{J_m(\lambda_{mn} a)}\right) = \frac{1}{2}\omega^2 \mathfrak{N}(W_{n\alpha} - R_{n\alpha}),$$

or that

$$W_{n\alpha} - R_{n\alpha} = \frac{2\Omega_n^2 L_0}{\omega^2 \mathfrak{N}} \left(\frac{J_m(\lambda_{m\alpha} a)}{J_m(\lambda_{mn} a)}\right) C_{n\alpha}.$$

Noting that

$$\frac{\Omega_n^2 L_0}{\omega^2 \mathfrak{N}} = \frac{1}{4} a \lambda_n T_n = \frac{a}{4 s_n}$$

and that the expression for $C_{n\alpha}$ given by GFS (1992) (re-written in the present notation) for $n \neq \alpha$ is

$$C_{n\alpha} = \frac{2m^2 \lambda_n^2 (s_\alpha - s_n)}{(\lambda_n^2 a^2 - m^2)(\lambda_n^2 - \lambda_\alpha^2) a}$$

the equality follows easily.

Other coefficients: The $Q_{n\alpha\beta}$, and R_{np} coefficients have to be calculated using numerical integration.

Appendix C. Coefficients for the narrow annulus

The eigenfunctions are given by

$$E_n^m = \mathrm{e}^{\mathrm{i}m\theta} \cos\left(\frac{n\pi x}{L}\right), \quad n = 0, 1, 2, \ldots, \quad \left\|E_n^m\right\|^2 = \pi a L(1 + \delta_{n0}),$$

where $x = r - a$. The corresponding eigenvalues are

$$\lambda_{mn}^2 = \frac{m^2}{a^2} + \left(\frac{n\pi}{L}\right)^2.$$

The torsion function takes the simple approximate form, $T = -\frac{1}{2}ax$, and the first-order solution coefficients are given by,

$$\Gamma_n = \frac{aL}{n^2\pi^2}\left(1 - (-1)^n\right), \qquad h_n = \frac{a[1 - (-1)^n] T_n}{8\lambda_n L[(\Omega_n^2/4\omega^2) - 1]}.$$

The $Q_{n\alpha\beta}^{mm0}$, or simply $Q_{n\alpha\beta}$, coefficients can be found, using the identity

$$E_n^{m*} E_\alpha^m = \frac{1}{2}\left(E_{|n-\alpha|}^0 + E_{n+\alpha}^0\right).$$

It follows that

$$Q_{n\alpha\beta} = \frac{1}{2(1+\delta_{n0})}\sigma_{n\alpha\beta},$$

where

$$\sigma_{n\alpha\beta} = \delta_{(n+\alpha+\beta)\,0} + \delta_{(n+\alpha-\beta)\,0} + \delta_{(n-\alpha+\beta)\,0} + \delta_{(n-\alpha-\beta)\,0}.$$

To find the W coefficient, first note that,

$$S_{np} = 2\pi \mathrm{i}m\big((-1)^{n+p} - 1\big).$$

Also,

$$Z_{n\alpha} = -\frac{1}{2}\mathrm{i}m\delta_{n\alpha},$$

so

$$\frac{Z_{p\beta}S_{n\beta}F_{n\beta}}{\|E_n^m\|^2 s_n} = -\frac{m^2[1-(-1)^{n+p}]F_{np}}{aLs_n(1+\delta_{n0})},$$

$$R_{nn} = 0, \qquad R_{np} = \frac{n^2 a[1-(-1)^{n+p}]}{L(n^2-p^2)(1+\delta_{n0})} \quad (n \neq p).$$

To calculate T_{np} we first note that

$$\psi_n = \frac{\mathrm{i}m}{a}\sum_{k=0}^{\infty} a_{kn}X_{kn}(x)\cos(\mu_k x)\,\mathrm{e}^{\mathrm{i}m\theta},$$

where

$$X_{kn}(x) = \frac{(-1)^n\cosh\xi_k x - \cosh[\xi_k(L-x)]}{\xi_k\sinh(\xi_k L)},$$

and

$$\xi_k^2 = \mu_k^2 + \frac{m^2}{a^2}.$$

As before $\mu_k = k\pi/h$ and the a_{nk} are the coefficients in the Fourier cosine series expansion of $f_n(z)$.

It then follows that

$$-s_n T_{np}(1+\delta_{n0}) = \frac{2m^2}{a^2 Lh\lambda_n^2\lambda_{p^2}}\big[1+(-1)^{n+p}\big]\frac{c_0-(-1)^p}{\xi_0\sinh(\xi_0 L)} + \frac{4m^2}{a^2 Lh}\big[1+(-1)^{n+p}\big]\sum_{k=1}^{\infty}\frac{[c_k-(-1)^p]}{\xi_k\sinh(\xi_k L)(\lambda_p^2+\mu_k^2)(\lambda_n^2+\mu_k^2)},$$

where $c_k = \cosh(\xi_k L)$.

Appendix D. Formula for Q'_{pqr}

We begin by using the identity $\nabla^2 E_r = -\lambda_r^2 E_r$ to derive the formula,

$$\nabla\cdot(E_p E_q \nabla E_r) = -\lambda_r^2 E_r E_p E_q + E_p\nabla E_q\cdot\nabla E_r + E_q\nabla E_p\cdot\nabla E_r.$$

Integrating over the cross-section, and applying the divergence theorem to the LHS we find

$$Q'_{pqr} = \lambda_r^2 Q_{pqr} - Q'_{qrp}. \tag{D.1}$$

Applying (D.1) to the last term on its right-hand side we obtain

$$Q'_{pqr} = \lambda_r^2 Q_{pqr} - \lambda_p^2 Q_{qrp} + Q'_{rpq}.$$

Repeating the process:

$$Q'_{pqr} = \lambda_r^2 Q_{pqr} - \lambda_p^2 Q_{qrp} + \lambda_q^2 Q_{rpq} - Q'_{pqr}$$

and rearranging, we find

$$Q'_{pqr} = \frac{1}{2}(\lambda_r^2 + \lambda_q^2 - \lambda_p^2) Q_{pqr}.$$

Acknowledgements

ADS gratefully acknowledges support from the Institut National Polytechnique de Grenoble, and the hospitality of the Madylam laboratory, June–August 2000.

References

[1] J.M. Galpin, Y. Fautrelle, Liquid-metal flows induced by low-frequency alternating magnetic fields, J. Fluid Mech. 239 (1992) 383–408.
[2] J.M. Galpin, Y. Fautrelle, A.D. Sneyd, Parametric resonance in low-frequency magnetic stirring, J. Fluid Mech. 239 (1992) 409–427.
[3] Y. Chino, K. Iwai, S. Asai, Control of free surface shape on a molten metal by synchronous imposition of a mechanical oscillation and intermittent alternating magnetic field, in: Proceedings of the 3rd International Symposium on Electromagnetic Processing of Materials, Nagoya, Japan, April 3–6, 2000, The Iron and Steel Institute of Japan, Tokyo, 2000, pp. 49–54.
[4] M. Burty, J.M. Galpin, Y. Fautrelle, F. Debray, T. Inomoto, Y. Ogawa, T. Toh, I. Sawada, K. Harashima, Contribution to fundamental study of metal-slag mass transfer in ladle metallurgy, in: Proceedings of the 3rd International Symposium on Electromagnetic Processing of Materials, Nagoya, Japan, April 3–6, 2000, The Iron and Steel Institute of Japan, Tokyo, 2000, pp. 321–326.
[5] L.D. Landau, E.M. Lifshitz, Theory of Elasticity, Pergamon Press, Oxford, 1985.
[6] G.K. Batchelor, An Introduction to Fluid Dynamics, Cambridge University Press, 1965.
[7] A.D. Sneyd, A. Wang, Interfacial instability due to MHD mode coupling in aluminium reduction cells, J. Fluid Mech. 263 (1994) 343–359.
[8] A.D. Sneyd, Analysis of parametric resonance in magnetohydrodynamics, Eur. J. Mech. B Fluids (2002), in press.
[9] F. Debray, Y. Fautrelle, Electromagnetically driven parametric instability in an annular layer, in: F.T.M. Nieuwstadt (Ed.), Advances in Turbulence IV, in: Appl. Sci. Res., vol. 51, Kluwer Academic, 1993, pp. 31–36.
[10] J. Miles, On surface waves with zero contact angle, J. Fluid Mech. 245 (1992) 485–492.
[11] L.M. Hocking, The damping of capillary-gravity waves at a rigid boundary, J. Fluid Mech. 179 (1987) 253–266.
[12] T.B. Benjamin, F. Ursell, The stability of the plane free surface of a liquid in vertical periodic motion, Proc. Roy. Soc. London 225 (1954) 505–515.
[13] J.M. Galpin, Etude du couplage entre un métal liquide et un champ magnetique alternant a basse frequence. Ph.D. thesis, Institut National Polytechnique de Grenoble, France, 1992.
[14] F. Debray, Déformations d'interface engendrées par une excitation électromagnétique basse fréquence et mesure des transferts de masse associés, Thèse de doctorat, Institut National Polytechnique de Grenoble, 1994.